



Last glacial millennial-scale hydro-climate and temperature changes in Puerto Rico constrained by speleothem fluid inclusion $\delta^{18}\text{O}$ and $\delta^2\text{H}$ values

Sophie F. Warken^{1,2,★}, Therese Weißbach^{1,3,★}, Tobias Kluge^{1,3,4}, Hubert Vonhof⁵, Denis Scholz⁶, Rolf Vieten⁷, Martina Schmidt¹, Amos Winter^{7,8}, and Norbert Frank¹

¹Institute of Environmental Physics, University of Heidelberg, Heidelberg, Germany

²Institute of Earth Sciences, University of Heidelberg, Heidelberg, Germany

³Heidelberg Graduate School of Fundamental Physics, Heidelberg University, Heidelberg, Germany

⁴Institute of Applied Geosciences, Karlsruhe Institute of Technology, Karlsruhe, Germany

⁵Max Planck Institute for Chemistry, Climate Geochemistry Department, Mainz, Germany

⁶Institute for Geosciences, University of Mainz, Mainz, Germany

⁷Department of Marine Sciences, University of Puerto Rico, Mayagüez, Puerto Rico

⁸Earth and Environmental Systems Department, Indiana State University, Terre Haute, Indiana, USA

★These authors contributed equally to this work.

Correspondence: Sophie F. Warken (swarken@iup.uni-heidelberg.de)

Received: 9 July 2021 – Discussion started: 30 July 2021

Revised: 15 December 2021 – Accepted: 4 January 2022 – Published: 1 February 2022

Abstract. We present speleothem fluid inclusion $\delta^{18}\text{O}_f$ and $\delta^2\text{H}_f$ values from Larga Cave, Puerto Rico, that cover the interval between 46.2 and 15.3 ka on the millennial scale, including the Last Glacial Maximum (LGM) and several stadial and interstadial cycles. The data set can be divided in two main clusters of stable isotope compositions of the fluid inclusion water with respect to the global meteoric water line (GMWL), which coincide with strong variations in the water content of the stalagmite. In particular, this clustering is found to be climate related, where one cluster comprises samples from cold and dry periods, such as the Heinrich and Greenland stadials (HSs and GSs), as well as parts of the LGM, which exhibit very high $\delta^{18}\text{O}_f$ and $\delta^2\text{H}_f$ values. We interpret this enrichment as being caused by evaporation inside the cave due to enhanced cave ventilation during these colder and drier times. In contrast, in most samples corresponding to warmer and wetter Greenland interstadials (GIs), but also for some from HS 2 and 3, the $\delta^{18}\text{O}_f$ and $\delta^2\text{H}_f$ values plot on the meteoric water line and modification of fluid inclusion water due to “in-cave” evaporation are found to be negligible.

Consequently, variations of recent glacial hydro-climate and temperatures in the western tropical Atlantic can be con-

strained. In general, $\delta^{18}\text{O}_f$ values from fluid inclusions are up to 3‰ higher than those of modern drip water, which is interpreted as a weaker atmospheric convective activity during the last glacial period. In addition, reconstructed temperatures suggest an average cooling of 2–3 °C during the LGM compared to modern cave temperatures. Reconstructed cave temperatures yield an average cooling of -1.4 ± 2.8 °C for HS 2 and -3.6 ± 2.2 °C for HS 3. Higher $\delta^{18}\text{O}_f$ values of these samples further suggest that the drip water was dominated by orographic rainfall and/or cold fronts, along with weak or even absent convective activity. In contrast, during interstadial phases, reconstructed temperatures reached nearly modern values, and convective activity was comparable to or only slightly weaker than today.

1 Introduction

Stable isotopes of oxygen (represented by $\delta^{18}\text{O}$ values) are a widely used proxy used to deduce information about past climates from speleothems, since the cave drip water reflects the amount- or recharge-weighted annual mean isotopic signature of the rainfall above the cave (Baker et al.,

2019; Lachniet, 2009). This value is in turn modulated by several variables, such as temperature, the type and seasonal distribution of precipitation, and the source moisture trajectory (Lachniet, 2009; Bird et al., 2020; Lases-Hernandez et al., 2020). In the tropics, the isotopic composition of precipitation, $\delta^{18}\text{O}_p$, has been attributed to changes in precipitation amount and convective activity (Dansgaard, 1964; Lachniet and Patterson, 2009; Vieten et al., 2018a). Consequently, tropical speleothem $\delta^{18}\text{O}$ values are usually interpreted in terms of this isotopic “amount effect” (Medina-Elizalde et al., 2010; Arienzo et al., 2019; Lases-Hernandez et al., 2019). However, in the soil and karst above caves and at the surface of stalagmites, various (disequilibrium) isotope fractionation effects can obscure the interpretation of stable isotopes in speleothem calcite (Weber et al., 2021; Hansen et al., 2019; Carlson et al., 2020).

In this respect, stable isotopes of oxygen and hydrogen in speleothem fluid inclusions provide a useful proxy since these represent potentially unchanged aliquots of the original drip water, and thus relicts of past precipitation (Schwarcz et al., 1976; van Breukelen et al., 2008; Affolter et al., 2015). The utility of speleothem fluid inclusion analysis improves if the conditions of carbonate precipitation are well understood, i.e. whether or not the minerals precipitated close to “equilibrium conditions”. In the case of equilibrium conditions, palaeo-temperatures can be reconstructed from the combined oxygen isotope ratios of the calcite ($\delta^{18}\text{O}_c$) and the fluid inclusions, $\delta^{18}\text{O}_f$, based on known temperature-dependent isotope fractionation relationships between calcite and water (e.g. Kim and O’Neil, 1997; Tremaine et al., 2011; Hansen et al., 2019; Johnston et al., 2013). In continental mid- and high-latitude locations, estimation of palaeo-temperatures via fluid inclusion $\delta^2\text{H}_f$ values alone is feasible, based on the dominant control of temperature on rainfall isotope composition in such settings (Affolter et al., 2019; Demény et al., 2021). This only works, however, if the contribution of the amount effect is negligible. The analysis of speleothem fluid inclusions has been successfully applied worldwide, including tropical locations (Griffiths et al., 2010; Arienzo et al., 2015; Millo et al., 2017; Meckler et al., 2015). Nevertheless, speleothem fluid inclusion records from the Last Glacial Period (ca. 115–11.7 ka) are still sparse, and in many cases, reliable palaeo-temperature estimates are challenging (Millo et al., 2017; Demény et al., 2021; Nehme et al., 2020).

Here we present a detailed study of fluid inclusions from a Puerto Rican stalagmite (PR-LA-1), spanning the interval between 46.2 and 15.3 ka. The record encompasses a period which was characterized by rapid climatic fluctuations from cold (stadial) to warmer (interstadial) conditions recurring on millennial timescales (Dansgaard et al., 1984; Peterson et al., 2000). In palaeoclimate records from the tropics, the Heinrich stadials (HS) are clearly represented by dramatic cooling and dry conditions in the western tropical Atlantic (Escobar et al., 2012; Arienzo et al., 2015; Grauel et al., 2016).

These conditions were likely caused by a southward shift of the Inter-Tropical Convergence Zone (ITCZ) induced by a near shutdown of the Atlantic Meridional Overturning Circulation (AMOC; Broccoli et al., 2006; Lynch-Stieglitz et al., 2014; Deplazes et al., 2013; Escobar et al., 2012). Conversely, during the interstadials, the ITCZ was presumably in a more northerly position, accompanied by warmer and wetter climatic conditions and higher sea surface temperatures (SSTs) in the (sub-)tropical Atlantic (Schmidt et al., 2006a; Peterson et al., 2000; Sachs and Lehman, 1999).

The speleothem PR-LA-1 was selected because its stable isotope values ($\delta^{18}\text{O}_c$ and $\delta^{13}\text{C}_c$) and Mg / Ca ratios demonstrated a pronounced response to the local hydro-climate on the millennial scale (Warken et al., 2020). To further elucidate the millennial-scale climate changes during the last glacial stadials and interstadials, we thus conducted a large number of fluid inclusion measurements following prominent $\delta^{18}\text{O}_c$ changes in stalagmite PR-LA-1.

2 Material and Methods

2.1 Site description

Larga Cave (18°19' N, 66°48' W; Fig. 1) is located 350 m above sea level in the north central karst region of Puerto Rico. The overburden of Larga Cave is comprised of the Oligocene Lares limestone Fm., which is covered by a thin layer of soil. The host rock is exposed in some places, and the present-day vegetation consists of dense tropical forest. The main passage in the cave is almost horizontal and has a total length of 1400 m with a ceiling height of up to 30 m (Miller, 2010). Stalagmite PR-LA-1 has a total length of 185 cm and was found lying on the cave floor in the main passage, where the rock overburden is 40 to 80 m thick. The stalagmite was deposited between 15.4 and 46.2 ka, with a hiatus between 35.5 and 41.1 ka (Fig. 1; Warken et al., 2020). Microscopic inspection of thin sections shows that PR-LA-1 consists of calcite in columnar fabric and shows no signs of dissolution and/or recrystallization (Fig. S1). Between 2012 and 2017, the mean annual air temperature at the location of the cave was 22.5 °C, and the measured mean local annual rainfall was 2200 mm (Vieten et al., 2018a). Since 2012, cave air parameters, such as temperature (T), $p\text{CO}_2$, and relative humidity (RH), have been recorded at the location of stalagmite PR-LA-1. During this time, the cave temperature has been constant with values of 22.5 ± 0.2 °C. The cave air $p\text{CO}_2$ varies depending on the season, with high values of up to 1800 ppm in summer and low values of around 550 ppm in winter (Vieten et al., 2016). This seasonal pattern results from a temperature-driven, very well-ventilated cave environment in winter and low ventilation in summer. During the winter season, a high buoyancy contrast at night leads to maximal cave ventilation, while it is at a minimum during summer, when cave temperatures are lower than in the outside environment. RH is generally close to 100 %, but has

been found to decrease to values to 90%–95% for several weeks when ventilation intensifies in winter months (Vieten et al., 2016, 2018a).

As typical for Caribbean locations, the precipitation regime over Larga Cave is characterized by a drier winter season, from December to April and a much wetter season during the rest of the year. During the drier season, occasional light showers occur imbedded in trade winds, which are interrupted by occasional cold fronts emanating from North America (Scholl and Murphy, 2014). In contrast, during the remainder of the year convective rain is formed by easterly moving low pressure systems which occasionally develop into tropical depressions accounting for the majority of total precipitation (Scholl and Murphy, 2014). On inter-annual timescales, the $\delta^{18}\text{O}$ values of rainfall in Puerto Rico show a negative correlation with precipitation, suggesting an isotopic amount effect of ca. -0.1‰ per 100 mm of rainfall amount (Govender et al., 2013; Scholl et al., 2014; Warken et al., 2020). Over the course of monthly drip water monitoring (2013–2017), the drip water composition at sites with a maximum distance of 10 m to the location where stalagmite PR-LA-1 was found shows only little seasonal variation, with a mean value of $\delta^{18}\text{O}_w = -2.6 \pm 0.3\text{‰}$, and $\delta^2\text{H}_w = -9.5 \pm 0.2\text{‰}$ Vienna Standard Mean Ocean Water (VSMOW). The seasonal signal in the rainwater is strongly smoothed by the soil and epikarst above the cave with a mixing time of at least several months to years, suggesting that the Larga speleothem time resolution record is at least inter-annual.

A LMWL is available for three stations in Puerto Rico (Fig. 1). At San Agustín, located closest to Larga Cave, a monthly data set covering 1998 to 2012 shows a LMWL of $\delta^2\text{H} = 8.4 \times \delta^{18}\text{O} + 11.6\text{‰}$ (VSMOW; Putman et al., 2019; Scholl et al., 2014). Similar LMWLs (Fig. 1) exist for a site in the Luquillo Mountains in eastern Puerto Rico (Scholl and Murphy, 2014) and for the Guánica Dry Forest, located in south-western Puerto Rico (Govender et al., 2013).

2.2 Fluid inclusion stable isotope composition

Solid samples for fluid inclusion isotope analysis were cut using a band saw along the growth axis of stalagmite PR-LA-1. High growth rates of this specimen of up to 1 mm yr^{-1} allow for the sampling of distinct millennial-scale climate oscillations evident in the $\delta^{18}\text{O}_c$ record, such as D/O or Heinrich events. Replicate samples were taken along the corresponding growth layers to minimize the effect of integrating over too-long time intervals. Individual sample sizes were between 0.21 and 1.34 g. The speleothem fragments were placed in a copper tube and installed in a preparation line connected to a cavity ring down spectrometer (CRDS, L2130-I, Picarro) at the Institute of Environmental Physics, Heidelberg University (Weißbach, 2020). After connecting the sample, the setup requires approximately 90 min until the water vapour background has reached stable conditions.

When the standard deviation of the water vapour concentration is below 20 ppmV over 30 min, the sample is crushed with a hydraulic crusher. To avoid the CRDS memory effect, a stable water vapour background was generated to ensure constant saturation of the cavity without condensation (Affolter et al., 2014; De Graaf et al., 2020). This was achieved by mixing dry nitrogen as a carrier gas with water of a known isotopic composition, while the line, including the tube that holds the sample, was held at a constant temperature of 120°C .

The mixture of background water and sample signal is measured in the CRDS analyser, and evaluated similarly to the method of Affolter et al. (2014) with a Python code (Hemmer, 2022). The isotopic composition and released water volume are calibrated with in-house water standards and glass capillaries with known volumes in the microlitre range respectively. These are inserted into the copper tube and connected to the preparation line, similarly as the speleothem samples. The in-house water standards are analysed regularly against the international primary reference material Vienna Standard Mean Ocean Water 2 (VSMOW2) and Standard Light Antarctic Precipitation 2 (SLAP2). The long-term precision of single stable isotope measurements is 0.5‰ for $\delta^{18}\text{O}$ and 1.5‰ for $\delta^2\text{H}$, while for released water volumes above $1.0\text{ }\mu\text{L}$, the precision improves to 0.2‰ for $\delta^{18}\text{O}$ and 0.4‰ for $\delta^2\text{H}$ (Weißbach, 2020). In the case of water volumes $< 0.2\text{ }\mu\text{L}$, the result of a single measurement may become less precise and is therefore reproduced by replicate measurements to verify the result. If not stated differently, the stable isotope composition of fluid inclusions is given relative to VSMOW.

3 Results

3.1 Water content and stable isotope composition of speleothem fluid inclusions

In total, 64 fluid inclusion water isotope measurements were performed at 30 different depth intervals. The results of the single measurements are shown in Table S1 in the Supplement, while the mean values of the replicate measurements are given in Table S2. The mean water content of PR-LA-1 calcite for the different depth intervals shows a variation of close to 0 to $3\text{ }\mu\text{L g}^{-1}$ (Fig. 2). Sections with a relatively high water content, e.g. around ca. 24 or 28 ka, also show a high (or at least highly variable) growth rate, while comparably low water content, such as at ca. 20, 26, or 32 ka, are mainly found in sections with relatively slow growth rates. The mean fluid inclusion water $\delta^{18}\text{O}_f$ values vary between -1.9 and $+11.4\text{‰}$, and mean $\delta^2\text{H}_f$ values are between $+6.9$ and $+44.9\text{‰}$ (VSMOW; Fig. 3a). The data exhibit a systematic ^{18}O and ^2H enrichment compared to modern drip water stable isotope values. This general pattern is also reflected in the slope of the linear regression line fitted to the data, which is with 2.42 ± 0.25 , significantly lower than expected

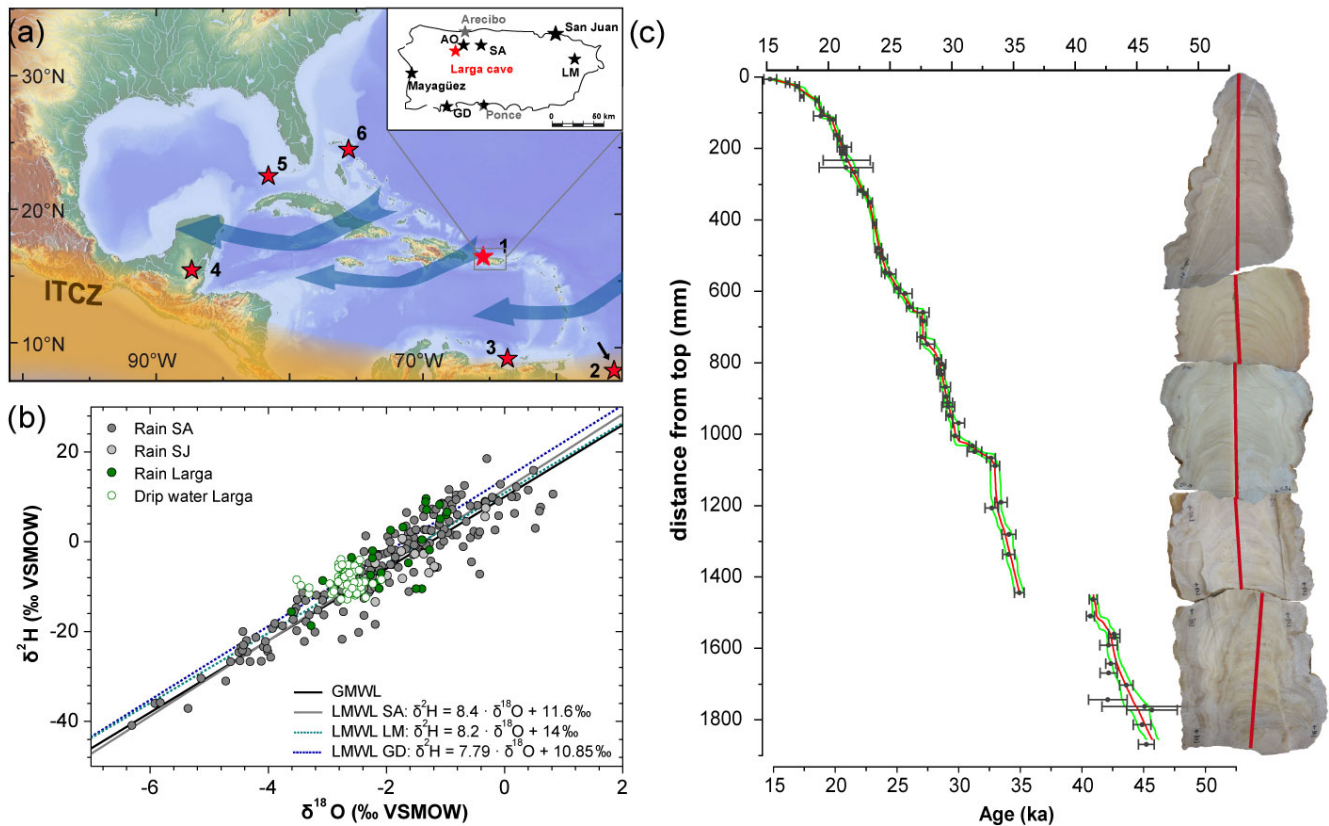


Figure 1. Sample locations and previous work on stalagmite PR-LA-1. (a) Location of Larga Cave (1), Puerto Rico, in the western tropical Atlantic region and other sites discussed in this study (map after Warken et al., 2020): (2) Guiana Basin (Rama-Corredor et al., 2015); (3) Cariaco Basin, Venezuela (Deplazes et al., 2013); (4) Lake Petén Itzá, Guatemala (Escobar et al., 2012; Grauel et al., 2016); (5) Florida Strait (Them II et al., 2015); (6) Abaco, Bahamas (Arienzo et al., 2015). The insert shows a detailed view of the location of Larga Cave (red star), and the position of local meteorological stations: Arecibo Observatory (AO), San Agustín (SA), Luquillo Mountains (LM), and Guánica Dry Forest (GD). Blue arrows in panel (a) indicate the dominant moisture trajectories over the region in boreal summer, when the ITCZ (yellow shaded area) is in its northernmost position. (b) Local rainwater isotope data from Larga Cave (Vieten et al., 2018b), SA (Scholl et al., 2014) and Global Network of Isotopes in Precipitation (GNIP) station San Juan (SJ). In addition, the global meteoric water line (GMWL) and local meteoric water line (LMWLs) are shown from SA (Putman et al., 2019; Scholl et al., 2014); LM (Scholl and Murphy, 2014) and GD (Govender et al., 2013). (c) Image of stalagmite PR-LA-1 and age–depth model from Warken et al. (2020).

for a LMWL. This slope agrees with those of globally distributed evaporation lines for lakes and soil waters (Gibson et al., 2008), as well as evaporation experiments (Hu et al., 2009).

Furthermore, the data can be allocated to two different clusters, depending on the measured water content of the samples. The first cluster comprises samples which are mainly located on or scatter around the GMWL. Most of these are also characterized by a water content greater than $0.55 \mu\text{L g}^{-1}$. In contrast, many samples show more positive $\delta^{18}\text{O}$ and $\delta^2\text{H}$ values and clearly plot off the GMWL along the linear regression line. In contrast to the first set of samples, most of these have a water content lower than $0.55 \mu\text{L g}^{-1}$. Only one sample clearly does not fit into this pattern and plots away from the GMWL despite a water content of $> 0.55 \mu\text{L g}^{-1}$ (sample 32b), which is therefore also allocated to cluster (2). Conversely, two samples plot close

to the MWLs despite a relatively low water content (samples 5 and 8). The relationship between fluid inclusion stable isotope values and water content is also expressed numerically with a negative correlation of $\delta^{18}\text{O}_f$ and the measured water content, with $r = -0.72$ ($r^2 = 0.51$) for logarithmic fitting (Fig. S2).

3.2 Calculation of palaeo-temperatures using the oxygen isotope equilibrium thermometer

In order to assess the applicability of the oxygen isotope equilibrium thermometer based on the mean fluid inclusion $\delta^{18}\text{O}_f$ values, the average carbonate $\delta^{18}\text{O}_c$ values were calculated from the intervals covered by the depth range of the measured fluid inclusion samples respectively (Table S2). Figure 4a shows that the previously mentioned pattern with two clusters of samples is also reproduced when compar-

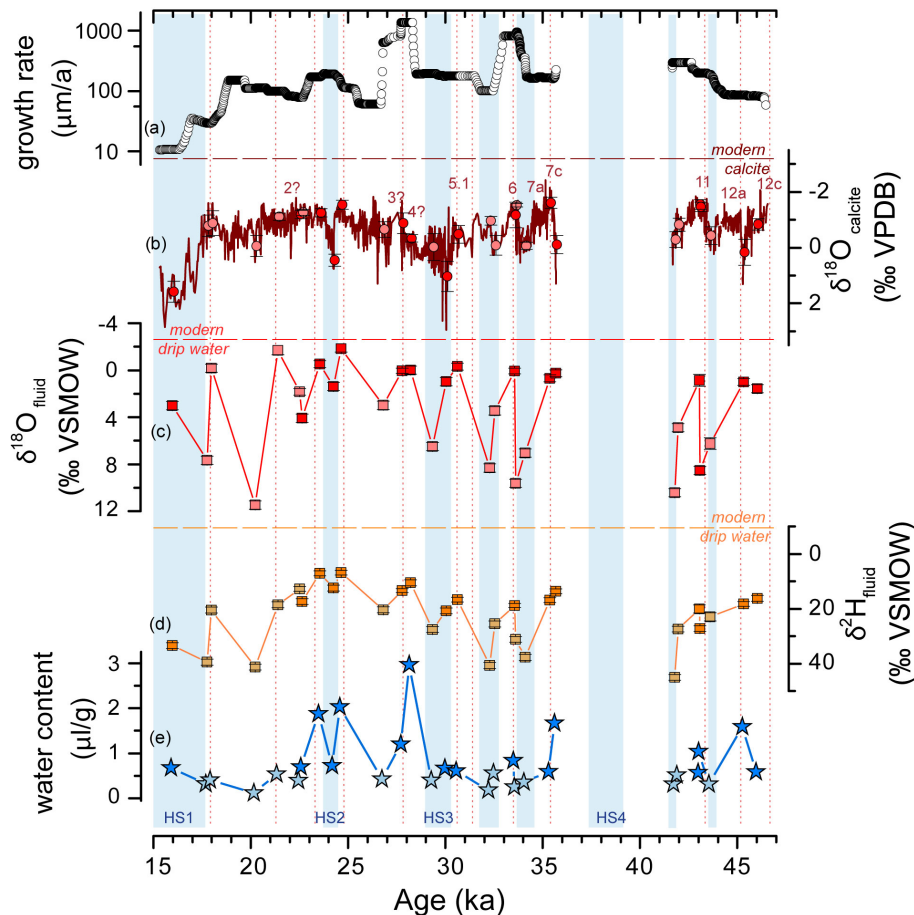


Figure 2. Results of fluid inclusion analysis of stalagmite PR-LA-1 (Table S2). From top to bottom: (a) growth rate (logarithmic scale) and (b) $\delta^{18}\text{O}_c$ values from Warken et al. (2020). Symbols indicate the averaged $\delta^{18}\text{O}_c$ values used for each depth of fluid inclusion isotope analysis respectively. Vertical blue bars (dotted red lines) indicate the timing of cool/dry (warm/humid) periods, such as HS 1 to 3 (Greenland interstadials (GIs) 12c to 6) in the western tropical Atlantic (Warken et al., 2020). The following panels show fluid inclusion isotope values of (c) $\delta^{18}\text{O}_f$, (d) $\delta^2\text{H}_f$, and (e) measured water content. Symbol colours indicate the samples with high (dark coloured symbols) and low (light coloured stars) water content, with a threshold value of $0.55 \mu\text{L g}^{-1}$ respectively. Horizontal lines indicate modern cave conditions. Note that the axes of the $\delta^{18}\text{O}_c$, $\delta^{18}\text{O}_f$, and $\delta^2\text{H}_f$ values are inverted.

ing the fluid inclusion $\delta^{18}\text{O}_f$ with the carbonate $\delta^{18}\text{O}_c$ values. Samples with high water content, which plot on the GMWL in Fig. 3a, are clearly separated by the samples with lower water content. While cluster (1) samples with high water content show a positive correlation between $\delta^{18}\text{O}_c$ and $\delta^{18}\text{O}_f$ values, cluster (2) samples do not follow the same trend. Similarly, the fractionation between speleothem calcite and fluid inclusions, $^{18}\epsilon_{c/f} = 1000 \times \ln \alpha$ (with $\alpha = (1000 + \delta^{18}\text{O}_c)/(1000 + \delta^{18}\text{O}_f)$, and $\delta^{18}\text{O}_c$ and $\delta^{18}\text{O}_f$ in VSMOW), shows a clear dependence on the $\delta^{18}\text{O}_f$ value for the evaporated samples of cluster (2) (Fig. 4b), but shows no relationship with carbonate $\delta^{18}\text{O}_c$ values (Fig. 4c). In contrast, for cluster (1) samples, no relationship between $^{18}\epsilon_{c/f}$ and $\delta^{18}\text{O}_f$ values is observed (Fig. 4b). Figure 4 also suggests that fluid inclusion samples 9b, 32b, 27, 32, and 36 are also enriched in ^{18}O , and have to be allocated to cluster (2).

For a first-order temperature calculation from $^{18}\epsilon_{c/f}$, three different isotope fractionation relationships have been tested (Kim and O’Neil, 1997; Tremaine et al., 2011; Johnston et al., 2013). All results are listed in Table S2, where the given uncertainties of the palaeo-temperatures result from propagating the analytical error of the fluid inclusion measurements, as well as the range of the $\delta^{18}\text{O}_c$ calcite value due to dating and sampling uncertainty. All palaeo-temperatures reported and discussed in the main text are calculated using the Tremaine et al. (2011) equation, which has been developed from cave monitoring and modern speleothem calcite and yields realistic temperatures compared to the modern cave air temperature (Table S2). Note that we discard samples from the temperature discussion where replicate measurements exhibit a poor reproducibility in terms of largely variable water content and large isotopic differences, in order to focus on the most robust palaeoclimatic inferences (Table S2). Note

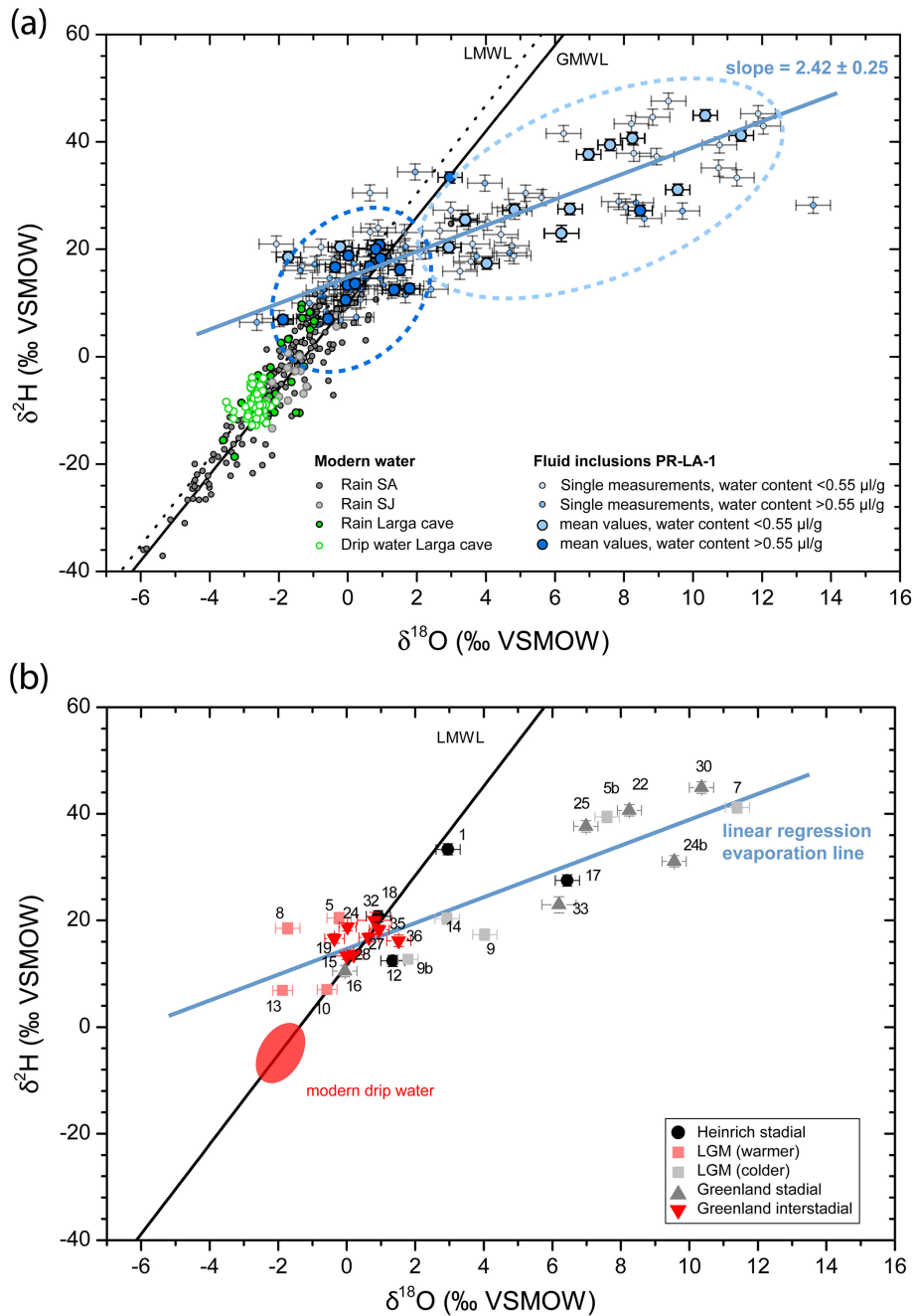


Figure 3. (a) Results of stable isotopes of fluid inclusions and drip waters in Larga Cave as indicated in Tables S1 and S2. Lines indicate the GMWL and the LMWL with $\delta^2\text{H} = 8.2 \times \delta^{18}\text{O} + 14\text{‰ VSMOW}$ by Scholl and Murphy (2014). Single values of the water isotopes in fluid inclusions (small circles) and mean values (large circles) with corresponding standard deviation are shown together with Larga Cave drip water from different drip sites (2013–2019, green triangles) and local rainwater data (compare Fig. 1). The mean values of the replicate measurements are allocated to two groups, with cluster (1) comprising samples on or scattering around the GMWL (indicated by the dark blue circle), and cluster (2) comprising all samples with a clear evaporation signal, plotting off the GMWL (light blue circle). (b) Stable isotope values of fluid inclusions from stalagmite PR-LA-1, categorized according to their allocation to the presumably warm (interstadial) or cold (stadial) periods when they formed. Thereby, a distinction is made between Heinrich stadials, Greenland stadials, and Greenland interstadials. Analysed samples from the LGM are also subdivided into presumably more warm/humid and relatively cool/dry periods. Numbers refer to the sample IDs as shown in Tables S1 and S2.

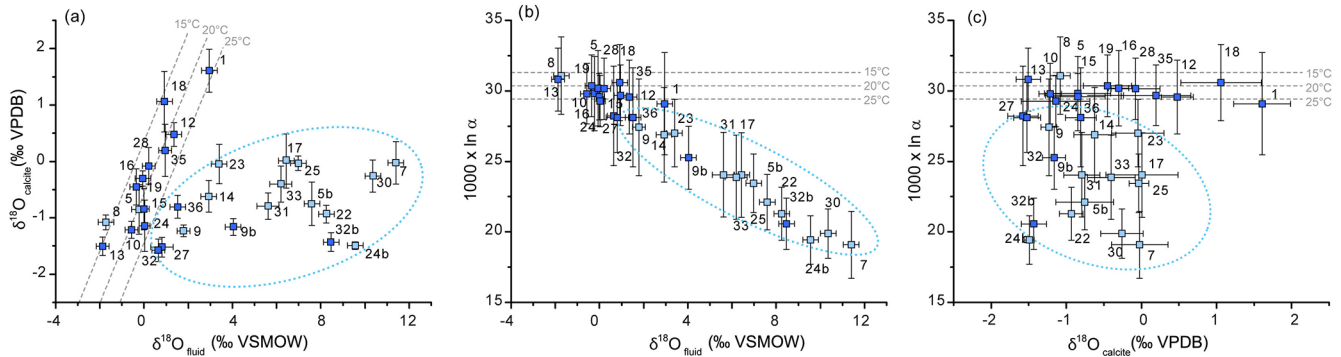


Figure 4. Analysis of the fractionation between speleothem calcite and fluid inclusions. Panel (a) shows the measured $\delta^{18}\text{O}_c$ values in speleothem carbonate (Warken et al., 2020) vs. measured $\delta^{18}\text{O}_f$ in speleothem fluid inclusion water (this study). (b) Fractionation $\delta_{c/f} = 1000 \ln \alpha$ between carbonate and fluid inclusion water vs. the $\delta^{18}\text{O}_f$ values. (c) Fractionation $1000 \ln \alpha$ vs. $\delta^{18}\text{O}_c$ values. Numbers indicate the sample IDs of the fluid inclusion measurements (Table S2). The uncertainty of the calculated fractionation is estimated from propagating the analytical error of the fluid inclusion measurements, and from the range of the $\delta^{18}\text{O}_c$ calcite value due to dating and sampling uncertainty. Blue symbols indicate samples with water content $> 0.55 \mu\text{L g}^{-1}$, and light blue symbols water content $< 0.55 \mu\text{L g}^{-1}$. The grey lines indicate the water–calcite oxygen isotope fractionation relationship after Tremaine et al. (2011) for cave temperatures of 15, 20 and 25 °C respectively. The ellipses indicate the samples which are allocated to cluster (2) due to large fractionation effects in $\delta^{18}\text{O}_f$. All of these samples also plot off the water–calcite oxygen isotope fractionation curve for 25 °C.

also that we do not report temperatures for samples of cluster (2), which clearly show significant influence from fractionation through evaporation (Table S2). We regard the temperature results obtained from the 12 replicate samples from cluster (1) as reliable within the large uncertainty of 1.5–2.5 °C. The calculated temperatures scatter around the modern cave temperature of 22.8 °C, with palaeo-temperatures varying between 16 ± 1.8 °C (sample 8, 21.39 ± 0.25 ka) and 25.7 ± 1.4 °C (sample 24, 33.52 ± 0.52 ka), and a mean value of 21.1 ± 2.7 °C.

4 Discussion

4.1 Influence of evaporation on PR-LA-1 fluid inclusion isotope data

4.1.1 Categorization of the fluid inclusion isotope data

For the fluid inclusion isotope data from cluster (1), $\delta^{18}\text{O}_f$ and $\delta^2\text{H}_f$ values scatter around the LMWL (Govender et al., 2013; Putman et al., 2019; Scholl and Murphy, 2014; Scholl et al., 2014). Thus, we suggest that these samples represent pristine fossil drip water. The second cluster of fluid inclusion isotope values mainly contains samples with water content below $0.55 \mu\text{L g}^{-1}$, which all show increased $\delta^{18}\text{O}_f$ values that are noticeably more fractionated than hydrogen isotopes. In addition to categorization with respect to water content, the fluid inclusion samples can be further associated with stadial and interstadial phases during the Last Glacial according to their stable isotope and elemental signatures in speleothem calcite (Fig. 3b). The fluid inclusion samples representing warm GIs (red triangle) plot close to the MWL and can be all associated with cluster (1). In con-

trast, the samples formed during the colder intervals (HS, GS, LGM) are mainly attributed to cluster (2) and trend away from the MWL. In addition, for Last Glacial Maximum (LGM) samples, the differentiation between the two clusters appears to be valid, with relatively warm/humid phases plotting closer to the MWL, and relatively dry/cool phases rather clustering with the GS and HS samples (Fig. 3b). This demonstrates that our data set allows us to distinguish cooler and/or drier climatic background states during the Heinrich and Greenland stadials, represented by cluster (2) samples, from the presumably warmer and more humid phases during the Greenland interstadials, which comprise cluster (1). Note that evaporation-driven fractionation must indicate a general annual decrease of humidity in the cave spanning decades that is required to trap the water in the calcite. Therefore, we suggest that samples of cluster (2) reflect periods with stronger cave ventilation as recorded presently in the thermal contrast of cave and ambient air in winter. This categorization suggests that the underlying process, which causes this clustering and affects the fluid inclusion isotopic signatures, is purely climate related.

Isotope effects due to the partial evaporation of fluid inclusion water can in principle also occur during the warm-up phase in the crusher when fluid inclusions are insufficiently sealed to withstand the pressure that builds up during warm-up. Based on our experience, water loss in the warm-up phase causes noticeable disruptions in the water background of the analyses, but this has been observed mostly for diagenetically compromised samples so far. We note that the water vapour background was continuously monitored before crushing, and no anomalies were observed in the samples from PR-LA-1 (Weißbach, 2020). Figure S1 also shows no

clear relationship between shape and distribution of fluid inclusions in PR-LA-1, nor do we see signs of diagenetic alteration in stalagmite PR-LA-1, which could have favoured inclusion leaking during heating. Previous studies have also invoked recrystallization-induced oxygen isotope changes in inclusion-hosted water of speleothems (Demény et al., 2016). This process is unlikely to be systematically related with climate and would shift the fluid inclusion $\delta^{18}\text{O}$ values towards more negative values, which is opposite to the observed pattern in this study.

Other studies suggest that in situ oxygen isotope exchange of fluid inclusion water with the host carbonate is unlikely to cause significant isotope fractionation (Uemura et al., 2020; Demény et al., 2021). The systematic enrichment of cluster (2) samples indicates that the stable isotope composition of the low water content samples has been affected by fractionation processes in the gas phase as ^{18}O is enriched over H isotopes, just as in non-equilibrium evaporation of thin water films (Gat et al., 1994). Thus, all information combined suggests evaporation inside the cave on the surface of the stalagmite as the scenario most likely to cause the lower slope of the water isotope relationship of 2.42 ± 0.25 (Fig. 3) via temperature- and humidity-related climate change (Gibson et al., 2008; Hu et al., 2009).

4.1.2 Climate-related evaporation effects on fluid inclusion isotope values in Larga Cave

Recent studies have suggested that in-cave evaporation may affect the isotopic composition of speleothem fluid inclusions (Nehme et al., 2020; Weißbach, 2020). A potential climate-related driver of this evaporative fractionation that has not been described previously is temperature-driven ventilation. This effect has been observed in Larga Cave, especially during the dry winter season (Vieten et al., 2016). Cave air ventilation may provoke evaporation of remaining water at the stalagmite's surface, which in turn influences the $\delta^{18}\text{O}_f$ and $\delta^2\text{H}_f$ values of the inclusion water seconds (Dreybrodt and Scholz, 2011; Deininger et al., 2012; Day and Henderson, 2011). At the same time, evaporation would also reduce the water content of the inclusions, explaining the systematically lower water content of cluster (2) samples (Sect. 3.1 and Fig. S2). Since speleothems are covered only by a thin film of water, evaporation can be very effective, especially given the high average cave temperature of Larga Cave and assuming a persistently lowered humidity. Calculation of the evolution of both water content and fluid inclusion $\delta^{18}\text{O}$ values with a Rayleigh fractionation approach (Fig. S2) supports this interpretation and shows that a moderate evaporation of 50 %–75 % of the initial water content (between 0.5 and $3 \mu\text{L g}^{-1}$) is sufficient to explain the observed enrichment of more than 12 ‰ of the fluid inclusion $\delta^{18}\text{O}_f$ values.

Figure 4 shows that the fractionation $^{18}\epsilon_{cf}$ between speleothem carbonate and fluid inclusion water is dominated by the enrichment of the fluid inclusion water, which

means that the process resulting in the large fractionation of the $\delta^{18}\text{O}_f$ values indeed only has a minor effect on the $\delta^{18}\text{O}_c$ values of CaCO_3 . When regarding both cluster (1) and cluster (2), $^{18}\epsilon_{cf}$ is largely independent from $\delta^{18}\text{O}_c$ values (Fig. 4c), while a very strong correlation with $\delta^{18}\text{O}_f$ values is evident (Fig. 4b). This argues for the significant influence of evaporation, which would have a strong effect on the fluid inclusion water, but only a minor effect on the precipitated carbonate. The reason for the different effect of evaporation on the $\delta^{18}\text{O}_f$ values of the fluid inclusion water and the precipitated calcite is related to the very different timescales of precipitation and oxygen isotope exchange between water and dissolved bicarbonate. Precipitation of calcite occurs on a timescale of a few hundred seconds (Dreybrodt and Scholz, 2011), depending – amongst other parameters – on cave temperature and film thickness. The timescale of oxygen isotope exchange between water and dissolved bicarbonate, in contrast, is in the range of hours to days (Beck et al., 2005; Dreybrodt and Scholz, 2011), and thus orders of magnitude longer.

When the drip water enters the cave, it is reasonable to assume that the $\delta^{18}\text{O}$ value of the dissolved bicarbonate is in oxygen isotope equilibrium with the $\delta^{18}\text{O}$ value of the drip water. When the drip water then falls onto the surface of a stalagmite, degassing of excess CO_2 occurs within a few seconds (Dreybrodt and Scholz, 2011), with a negligible effect on the $\delta^{18}\text{O}$ value of the dissolved bicarbonate. Then, precipitation of CaCO_3 starts immediately, and the $\delta^{18}\text{O}$ value of the bicarbonate that was previously equilibrated with the drip water is imprinted on the $\delta^{18}\text{O}$ value of the precipitated calcite. We note that oxygen isotope fractionation during precipitation of speleothem calcite is a complex process (e.g. Dreybrodt and Scholz, 2011; Guo and Zhou, 2019; Hansen et al., 2019; Scholz et al., 2009), and oxygen isotope fractionation does not, in most cases, occur under conditions of oxygen isotope equilibrium. After rapid precipitation of speleothem calcite, the drip water remaining on the surface of the speleothem, which forms the fluid inclusion water when it is eventually trapped, is progressively affected by evaporation, which leads to increasing $\delta^{18}\text{O}$ and $\delta^2\text{H}$ values of the water, and finally to fluid inclusions that are not in isotope equilibrium with the host-calcite. However, due to the very long time constant of oxygen isotope exchange between water and bicarbonate, it takes hours to imprint the oxygen isotope signature of the (evaporated) water on the dissolved HCO_3^- , and hence, the precipitated calcite. In addition, since the Ca concentration of the drip water drops exponentially, only a minor component of calcite could still be precipitated from the remaining solution (Scholz et al., 2009; Mühlinghaus et al., 2007; Deininger et al., 2012; Dreybrodt and Scholz, 2011). Given the smaller amount of Ca typically left in the solution, even under evaporative conditions, only an insignificant amount of calcite may be formed from the solution affected by evaporation. Thus, in the case of evaporation inside the cave, the $\delta^{18}\text{O}$ values of the precipitated calcite

would still reflect the $\delta^{18}\text{O}$ value of the original drip water, whereas the trapped fluid inclusion water may be strongly affected by evaporation and exhibit elevated $\delta^{18}\text{O}$ values (Fig. 3). These processes have been modelled by Deininger et al. (2012), who indeed predicted an enrichment of the $\delta^{18}\text{O}$ values of the water film on the surface of a stalagmite of several per mil due to evaporation, whereas the effect on the $\delta^{18}\text{O}$ values of the precipitated calcite was below 1‰.

Ventilation in Larga Cave is mainly driven by temperature differences between the atmosphere and the cave (Vieten et al., 2016). During the dry winter season, over the course of the day, the part of the cave hosting the studied speleothem is warmer than the atmosphere, inducing a buoyancy-driven air flow. According to our results, evaporation effects are strongest during the comparably cooler and drier periods of the record. This in turn suggests that cave ventilation was particularly pronounced in these times, which would argue for a stronger seasonal temperature contrast during stadial intervals. This observation is consistent with the hypothesis of enhanced Northern Hemisphere seasonality during abrupt cooling events (Denton et al., 2005). Similarly, Ziegler et al. (2008) reported persistently high summer temperatures of the Atlantic warm pool also during North Atlantic cold events, such as the Heinrich stadials, suggesting that these seem to influence mainly the winter climate conditions in the Caribbean. It is therefore plausible that a pronounced and persistently strong seasonal temperature difference with particularly cool temperatures during the winter season enhanced winter type ventilation conditions in Larga Cave. Hence, ventilation, and thus, the occurrence of evaporation on the stalagmite's surface would have been significant.

4.1.3 Applicability of the oxygen isotope equilibrium thermometer

The previously discussed processes have implications for the applicability of the oxygen isotope equilibrium thermometer using fluid inclusion and carbonate $\delta^{18}\text{O}$ values from PR-LA-1. Post-depositional (but pre-entrapment) enrichment of ^{18}O in fluid inclusion water due to evaporation apparently results in high $^{18}\epsilon_{\text{c/f}}$ fractionation values between fluid inclusion water and calcite, because such influenced samples do not preserve the original $\delta^{18}\text{O}_{\text{f}}$ signal. Samples plotting off the MWL are thus discarded from further inference. Note that evaporation effects would increase reconstructed temperatures by a factor of 2 to even 3; hence, temperature reconstruction is very sensitive to evaporation, which must be considered when interpreting meaningful temperature values as likely being maximum temperature estimates. Figure 4 shows that samples plotted on the GMWL in Fig. 3 might also show signs of evaporation. This is the case for the sample taken from HS 1 (15.9 ka). Here, other palaeoclimate records, as well as PR-LA-1 calcite $\delta^{18}\text{O}$ values and elemental proxies, suggest that this phase was the coolest and driest in Puerto Rico and the Caribbean realm (Warken et al.,

2020; Escobar et al., 2012; Grauel et al., 2016). The temperature calculated from the PR-LA-1 fluid inclusion value, however, is considerably warmer than at present day. As outlined above, we have to assume that evaporative effects also influenced speleothem and fluid inclusion formation during HS 1, shifting the $\delta^{18}\text{O}_{\text{f}}$ to heavier (more positive) values. This demonstrates that samples may be influenced from evaporation despite a position on or close to the MWL. We therefore consider all calculated temperatures as a maximum estimate, and results less than +3 °C greater than modern temperatures are considered, at first, plausible.

4.2 Reconstruction of hydro-climate and palaeo-temperatures in the western tropical Atlantic region

4.2.1 Fluid inclusion $\delta^{18}\text{O}$ values suggest reduced convective activity during the last glacial

Despite their position close to the MWL, $\delta^{18}\text{O}_{\text{f}}$ values in cluster (1) are significantly higher, by $+2.6 \pm 1.3\text{‰}$, compared to modern drip water $\delta^{18}\text{O}_{\text{w}}$. At the time of deposition of speleothem PR-LA-1 (46.2 to 15.3 ka), the $\delta^{18}\text{O}$ signature of the (sub)tropical Atlantic surface water was higher by about 1.5‰ due to larger global continental ice volume and increased salinity of the western tropical Atlantic (Hagen and Keigwin, 2002; Lea et al., 2003; Schmidt and Spero, 2011). Consequently, glacial drip water represented by fluid inclusion $\delta^{18}\text{O}_{\text{f}}$ values must be corrected for this 1.5‰ offset from the present day. Millo et al. (2017) reported a similar enrichment of about 4‰ compared to modern drip water in last glacial fluid inclusion water in a subtropical stalagmite from Brazil, and a similar glacial–interglacial offset has been observed in $\delta^{18}\text{O}$ values of stalagmites from Guatemala (Winter et al., 2020) and Florida (van Beynen et al., 2017).

We interpret the offset in cluster (1) as reflecting generally weaker convective activity during the last glacial period compared to modern conditions and associated reduced summer rainfall (e.g. Arienzo et al., 2019; Winter et al., 2020; Lasas-Hernandez et al., 2019, 2020; Bird et al., 2020). Today, rainfall in Puerto Rico is isotopically enriched when it is formed by occasional northerly cold fronts and the orographic processes of trade winds (Scholl and Murphy, 2014). In contrast, isotopically lighter precipitation is associated with convective rain, such as hurricanes and tropical storm events. The type of precipitation, i.e. convective vs. orographic, depends to some extent on the meridional location of the ITCZ and related Caribbean SSTs (Winter et al., 2020). In this study, the mean of the reconstructed fluid inclusion temperatures for the LGM (ca. 25–18 ka) is $20.6 \pm 3.2\text{ °C}$. Since our reconstructed temperatures can be regarded as upper limits, due to an underlying imperceptible amount of evaporation, this supports generally cooler temperatures than today over the course of the LGM. The observation of a glacial–interglacial temperature difference of 2–3 °C highlights previous results

of Caribbean SST records (Rama-Corredor et al., 2015; Lea et al., 2003; Schmidt et al., 2006b). Such low temperatures were presumably too cold to sustain strong convective activity during the LGM. Accordingly, Winter et al. (2020) suggested that deep atmospheric convection during the Holocene was triggered by exceeding an SST threshold of 27.5 °C in the tropical ocean, leading to a shift of the hydro-climatic regime from a drier state and weak convection during the last glacial to a humid state and strong convection after 9 ka over Central America.

The mean value of Puerto Rican fluid inclusion temperatures obtained during MIS 3 (45.5–29 ka) is 21.7 ± 2.6 °C. Despite the relatively large uncertainties, this may support a warmer MIS 3 than LGM, which has been found in the Guiana Basin (Rama-Corredor et al., 2015) and Brazil (Millo et al., 2017). For central Mexico, Caballero et al. (2019) report a mean annual temperature of MIS 3, comparable to the present day. From a global perspective, MIS 3 was ca. 2 °C warmer than the LGM, due to a northern hemispheric summer insolation maximum and the resulting smaller ice sheets (Van Meerbeek et al., 2009; Svendsen et al., 2004). According to Rama-Corredor et al. (2015), western tropical Atlantic SSTs were close to the threshold of 27.5 °C during certain intervals of MIS 3 (Fig. 5), allowing sustainment of convective activity at least temporarily and/or over a longer time interval over the course of the year. Consequently, relatively wet environmental conditions – even though still drier than those of the Holocene – are supported by records from Mexico, Guadeloupe and the Bahamas (Lozano-García et al., 2015; Royer et al., 2017; Arienzo et al., 2017).

4.2.2 Millennial-scale climate variability in the western tropical Atlantic

On the millennial scale, fluid inclusion $\delta^{18}\text{O}_f$ (and $\delta^2\text{H}_f$) values exert pronounced swings between very high values of up to 2‰ (30‰) during stadial phases and values down to 0‰ (15‰) during interstadial phases between 45 and 27 ka. The pattern largely follows the evolution of the high-resolution calcite stable isotope record (Fig. 2). Vertical blue bars in Figs. 2 and 5 illustrate the intervals of elevated $\delta^{18}\text{O}_c$ values during the Heinrich stadials, which are associated with relatively cold and dry conditions in the circum-Caribbean area. The upper limits calculated for palaeo-temperatures are between 17.4 ± 1.5 and 22.8 ± 1.6 °C for HS 2 and between 18.6 ± 1.9 and 19.8 ± 1.5 °C for HS 3 (Fig. 5, Table S2). Accordingly, we estimate an minimum average cooling compared to present-day cave air temperature of -1.4 ± 2.8 °C for HS 2 and -3.6 ± 2.2 °C for HS 3. These values are consistent with the results of Arienzo et al. (2015), who found an average temperature decrease of 4 °C across HS 1 to 3 for the Bahamas. In addition, many studies document that HS 1 exhibited the most pronounced cooling of all Heinrich stadials (Arienzo et al., 2015; Grauel et al., 2016). HS 1 was also more pronounced in the isotopic and elemental calcite signals

of our sample compared to HS 2 or 3 (Warken et al., 2020). Escobar et al. (2012) and Grauel et al. (2016) found an even stronger cooling, down to 10 °C for HS 1 in Lake Petén Itzá, Guatemala (Fig. 5). We note, however, that these studies used bottom dwelling ostracods, which may have recorded winter-biased lake temperatures. In addition, the strong maritime climate of Puerto Rico, located in the eastern Caribbean, makes less pronounced temperature variations appear reasonable. In addition to absolute temperature estimates, the samples which show signs of evaporation from cluster (2) suggest that during these times an increased seasonal temperature difference between persistently warm summer temperatures but cooler winter temperatures lead to enhanced cave ventilation. The timing of these samples, which includes not only the Heinrich stadials but also Greenland stadials and certain intervals of the LGM, is highlighted in Fig. 5. This further illustrates that our data set suggests that enhanced seasonality may have occurred during these intervals, which would be indicative of a persistent summer expansion of the Atlantic warm pool, but relatively cool winter temperatures.

Besides the temperature drops associated with Heinrich stadials, the expression of Greenland interstadials is still not well constrained in the American tropics (Warken et al., 2019). The mean temperature calculated from samples associated with interstadial events in speleothem PR-LA-1 is 22.8 ± 1.9 °C (samples 15, 24, 28, 35), which is in the range of the present-day cave temperature. In comparison to the average stadial temperatures of 19.7 ± 0.9 °C (samples 16, 18, 19), this indicates a difference of up to 3 °C between stadial and interstadial phases in Puerto Rico. In the tropical Guiana Basin, at 7° N latitude, abrupt glacial SST variations on the millennial scale are in the range of about ± 1 °C (Rama-Corredor et al., 2015). Further north, Them II et al. (2015) report a shift of ca. 2 °C associated with stadial/interstadial transitions in the Florida Strait (24° N), whereas shifts by 2 to 5 °C have been observed in subtropical SSTs, such as at the onsets of GI8 and GI12 at the Bermuda Rise at 33° N (Sachs and Lehman, 1999). Despite the large uncertainties associated with the oxygen isotope equilibrium thermometer, our results are thus consistent with these previous reconstructions and suggest that the interstadial phases in the western tropical Atlantic are also associated with relatively warm temperatures for Puerto Rico, and which may have been even comparable to the present day. Such warm temperatures favoured convective activity, and thus, higher precipitation amounts in the region. Marine reconstructions showed that interstadials were associated with reduced upper water column salinity, while stadial events were associated with increased salinity (Them II et al., 2015). These observations support our results that meridional shifts in the position of the ITCZ in response to changes in the strength of the AMOC affected the evaporation–precipitation ratio in the western tropical Atlantic (Schmidt and Spero, 2011; Arienzo et al., 2017; Peterson et al., 2000; Schmidt et al., 2006a; Warken et al., 2020).

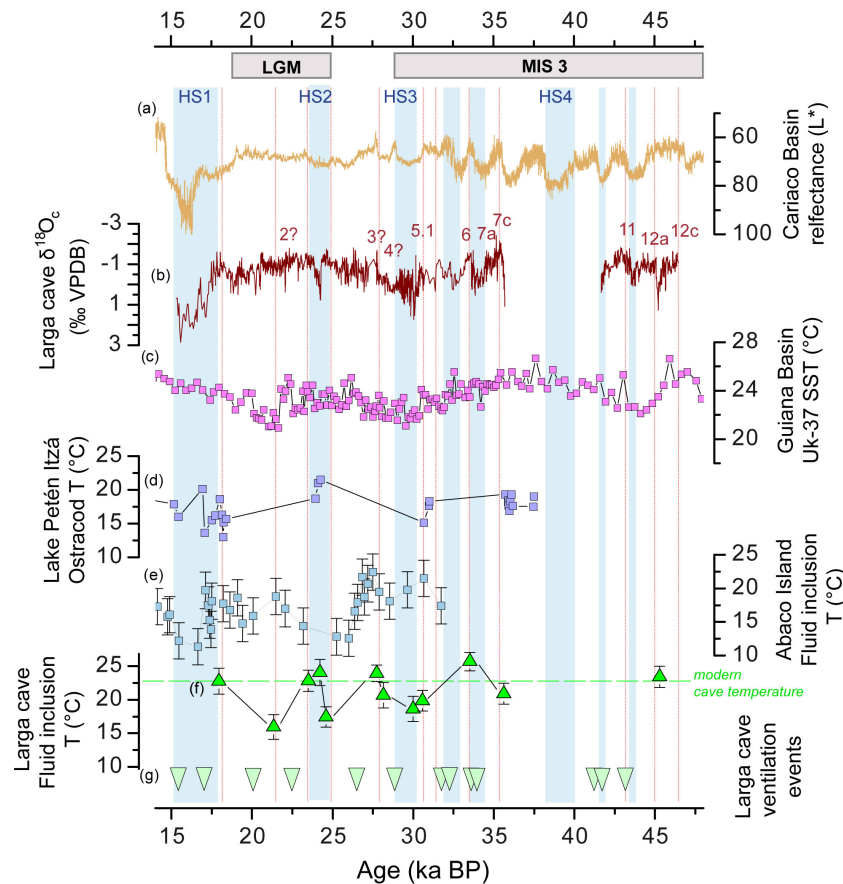


Figure 5. Palaeo-temperatures and the hydro-climate in the western tropical Atlantic region during the LGM and MIS2. From top to bottom: (a) Cariaco Basin reflectance record representing the mean meridional position of the ITCZ over northern South America (Deplazes et al., 2013); (b) speleothem PR-LA-1 $\delta^{18}\text{O}_e$ values from Warken et al. (2020), representing the local high-resolution hydro-climate; (c) Guiana Basin Uk37 SST reconstruction (Rama-Corredor et al., 2015); (d) Ostracod $\delta^{18}\text{O}$ -derived temperature record from Lake Petén Itzá (Guatemala; Escobar et al., 2012); (e) speleothem fluid inclusion-based temperature reconstruction from the Bahamas (Arienzo et al., 2015); (f) fluid inclusion-derived temperatures from PR-LA-1 (this study). The horizontal dashed line indicates modern cave air temperatures at Larga Cave. (g) Green triangles indicate the timing of Larga Cave ventilation events as suggested by fluid inclusion stable isotopic composition influenced by evaporation. In the tropical Atlantic, HS 1 to 4 and the Greenland stadials are associated with cold and dry conditions (light blue bars), and Greenland interstadials are associated with warmer and more humid climatic conditions (light red lines).

5 Conclusions

We demonstrate that the stable isotopic composition of fluid inclusions can be strongly influenced by evaporative effects. In Larga Cave, the temperature-driven ventilation potentially favoured such conditions, and our data suggest that this effect may have been especially pronounced during cold and dry conditions, such as during Heinrich and Greenland stadial phases and parts of the LGM. During warmer Greenland interstadials, most samples suggest that isotopic modification due to evaporation is negligible. In Larga Cave, this process is apparently climate related, making it possible to omit the potentially affected sub-samples for palaeo-temperature calculation.

Our data set thus provides valuable information about last glacial hydro-climate and temperature variability in the west-

ern tropical Atlantic and allows for constraining climatic changes on the millennial to orbital scale. For the presumably coldest phases of the last glacial, the Heinrich stadials, we observe a minimum cooling of $-1.4 \pm 2.8^\circ\text{C}$ during HS 2 and $-3.6 \pm 2.2^\circ\text{C}$ during HS 3. In contrast, during interstadial phases, temperatures were on average $23.4 \pm 1.7^\circ\text{C}$, which is comparable to modern values. The analysis of stable water isotope values in speleothem fluid inclusions further suggests that, compared to the present day, the precipitation regime in the western tropical Atlantic was characterized by generally weaker convective activity during the glacial period as compared to the present day. Especially during the LGM, average temperatures were 2–3 $^\circ\text{C}$ cooler, and thus too cold to sustain deep atmospheric convection. The intermediate background climate state during MIS 3 was potentially slightly warmer than the LGM, and favoured an increased

sensitivity of western tropical Atlantic hydro-climate to perturbations of the AMOC and northern hemispheric temperature changes on millennial scales. In this period, the region experienced significant shifts between a slightly weaker – but still active – convective regime during the warmer interstadial phases and a dry/non-convective regime during the colder stadial phases.

Code and data availability. The results of fluid inclusion isotope analyses from this study are available in the Supplement. The in-house Python code for the evaluation of the raw data is available under <https://github.com/bhemmer/IsoFluid> (last access: 28 January 2022; <https://doi.org/10.5281/zenodo.5911265>, Hemmer, 2022).

Supplement. The supplement related to this article is available online at: <https://doi.org/10.5194/cp-18-167-2022-supplement>.

Author contributions. SFW, TW, DS, and HV conceptualized the study. SFW and RV provided sample material and conducted field work. TW and SFW performed formal analysis, created the figures, and prepared the original draft. TW, SFW, RV, DS, and HV conducted the main investigations and data interpretation. Funding was acquired by TK, NF, MS, AW and DS. Methodology and resources were provided by TW, TK, MS, and NF. All authors reviewed and edited the final manuscript.

Competing interests. The contact author has declared that neither they nor their co-authors have any competing interests.

Disclaimer. Publisher's note: Copernicus Publications remains neutral with regard to jurisdictional claims in published maps and institutional affiliations.

Acknowledgements. Nicole Büttner, Marie C. Juhl, Nils Schorn-dorf, Ilona Fin, Oliver Wienand, and René Eichstädter are thanked for help in the lab and with sample preparation. Benedikt Hemmer is thanked for support in constructing the Python evaluation code. We further thank Thomas E. Miller, Augusto Mangini and Werner Aeschbach for ongoing support.

Financial support. This research has been supported by the Deutsche Forschungsgemeinschaft (grant nos. KL 2391/2–1, GSC129, INST 35_1143-1 FUGG, INST 35/1270-1 FUGG, SCHO 1274/6-1, SCHO 1274/9-1, and SCHO 1274/11-1) and the National Science Foundation (grant no. ATM-1003502).

Review statement. This paper was edited by Dominik Fleitmann and reviewed by two anonymous referees.

References

- Affolter, S., Fleitmann, D., and Leuenberger, M.: New online method for water isotope analysis of speleothem fluid inclusions using laser absorption spectroscopy (WS-CRDS), *Clim. Past*, 10, 1291–1304, <https://doi.org/10.5194/cp-10-1291-2014>, 2014.
- Affolter, S., Häuselmann, A. D., Fleitmann, D., Häuselmann, P., and Leuenberger, M.: Triple isotope (δD , $\delta^{17}\text{O}$, $\delta^{18}\text{O}$) study on precipitation, drip water and speleothem fluid inclusions for a Western Central European cave (NW Switzerland), *Quaternary Sci. Rev.*, 127, 73–89, 2015.
- Affolter, S., Häuselmann, A., Fleitmann, D., Edwards, R. L., Cheng, H., and Leuenberger, M.: Central Europe temperature constrained by speleothem fluid inclusion water isotopes over the past 14 000 years, *Sci. Adv.*, 5, eaav3809, <https://doi.org/10.1126/sciadv.aav3809>, 2019.
- Arienzo, M. M., Swart, P. K., Pourmand, A., Broad, K., Clement, A. C., Murphy, L. N., Vonhof, H. B., and Kakuk, B.: Bahamian speleothem reveals temperature decrease associated with Heinrich stadials, *Earth Planet. Sc. Lett.*, 430, 377–386, <https://doi.org/10.1016/j.epsl.2015.08.035>, 2015.
- Arienzo, M. M., Swart, P. K., Broad, K., Clement, A. C., Pourmand, A., and Kakuk, B.: Multi-proxy evidence of millennial climate variability from multiple Bahamian speleothems, *Quaternary Sci. Rev.*, 161, 18–29, <https://doi.org/10.1016/j.quascirev.2017.02.004>, 2017.
- Arienzo, M. M., Mehterian, S., Swart, P. K., Broad, K., and Kakuk, B.: Dripwater and Calcite Geochemistry Variations in a Monitored Bahamas Cave, *Geochem. Geophys. Geosy.* 20, 4306–4318, <https://doi.org/10.1029/2019gc008339>, 2019.
- Baker, A., Hartmann, A., Duan, W., Hankin, S., Comas-Bru, L., Cuthbert, M. O., Treble, P. C., Banner, J., Genty, D., and Baldini, L. M.: Global analysis reveals climatic controls on the oxygen isotope composition of cave drip water, *Nat. Commun.*, 10, 1–7, 2019.
- Beck, W. C., Grossman, E. L., and Morse, J. W.: Experimental studies of oxygen isotope fractionation in the carbonic acid system at 15°, 25°, and 40 °C, *Geochim. Cosmochim. Ac.*, 69, 3493–3503, 2005.
- Bird, M. I., Haig, J., Hadeen, X., Rivera-Araya, M., Wurster, C. M., and Zwart, C.: Stable isotope proxy records in tropical terrestrial environments, *Palaeogeogr. Palaeoclimatol.*, 538, 109445, <https://doi.org/10.1016/j.palaeo.2019.109445>, 2020.
- Broccoli, A. J., Dahl, K. A., and Stouffer, R. J.: Response of the ITCZ to Northern Hemisphere cooling, *Geophys. Res. Lett.*, 33, L01702, <https://doi.org/10.1029/2005gl024546>, 2006.
- Caballero, M., Lozano-García, S., Ortega-Guerrero, B., and Correa-Metrio, A.: Quantitative estimates of orbital and millennial scale climatic variability in central Mexico during the last ~40 000 years, *Quaternary Sci. Rev.*, 205, 62–75, 2019.
- Carlson, P. E., Noronha, A. L., Banner, J. L., Jenson, J. W., Moore, M. W., Partin, J. W., Deininger, M., Breecker, D. O., and Bautista, K. K.: Constraining speleothem oxygen isotope disequilibrium driven by rapid CO₂ degassing and calcite precipitation: Insights from monitoring and modeling, *Geochim. Cosmochim. Ac.*, 284, 222–238, <https://doi.org/10.1016/j.gca.2020.06.012>, 2020.
- Dansgaard, W.: Stable isotopes in precipitation, *Tellus*, 16, 436–468, 1964.

- Dansgaard, W., Johnsen, S. J., Clausen, H. B., Dahl-Jensen, D., Gundestrup, N., Hammer, C. U., and Oeschger, H.: North Atlantic climatic oscillations revealed by deep Greenland ice cores, *Climate Processes and Climate Sensitivity*, 29, 288–298, <https://doi.org/10.1029/GM029p0288>, 1984.
- Day, C. and Henderson, G.: Oxygen isotopes in calcite grown under cave-analogue conditions, *Geochim. Cosmochim. Ac.*, 75, 3956–3972, 2011.
- De Graaf, S., Vonhof, H. B., Weissbach, T., Wassenburg, J. A., Levy, E. J., Kluge, T., and Haug, G. H.: A comparison of isotope ratio mass spectrometry and cavity ring-down spectroscopy techniques for isotope analysis of fluid inclusion water, *Rapid Commun. Mass Sp.*, 34, e8837, <https://doi.org/10.1002/rcm.8837>, 2020.
- Deininger, M., Fohlmeister, J., Scholz, D., and Mangini, A.: Isotope disequilibrium effects: The influence of evaporation and ventilation effects on the carbon and oxygen isotope composition of speleothems – A model approach, *Geochim. Cosmochim. Ac.*, 96, 57–79, 2012.
- Demény, A., Czuppon, G., Kern, Z., Leél-Óssy, S., Németh, A., Szabó, M., Tóth, M., Wu, C.-C., Shen, C.-C., Molnár, M., Németh, T., Németh, P., and Óvári, M.: Recrystallization-induced oxygen isotope changes in inclusion-hosted water of speleothems – Paleoclimatological implications, *Quatern. Int.*, 415, 25–32, <https://doi.org/10.1016/j.quaint.2015.11.137>, 2016.
- Demény, A., Rinyu, L., Kern, Z., Hatvani, I. G., Gy, C., Surányi, G., Sz, L.-Ó., Shen, C. C., and Koltai, G.: Paleotemperature reconstructions using speleothem fluid inclusion analyses from Hungary, *Chem. Geol.*, 563, 120051, <https://doi.org/10.1016/j.chemgeo.2020.120051>, 2021.
- Denton, G. H., Alley, R. B., Comer, G. C., and Broecker, W. S.: The role of seasonality in abrupt climate change, *Quaternary Sci. Rev.*, 24, 1159–1182, 2005.
- Deplazes, G., Lückge, A., Peterson, L. C., Timmermann, A., Hamann, Y., Hughen, K. A., Röhl, U., Laj, C., Cane, M. A., Sigman, D. M., and Haug, G. H.: Links between tropical rainfall and North Atlantic climate during the last glacial period, *Nat. Geosci.*, 6, 213–217, <https://doi.org/10.1038/ngeo1712>, 2013.
- Dreybrodt, W. and Scholz, D.: Climatic dependence of stable carbon and oxygen isotope signals recorded in speleothems: From soil water to speleothem calcite, *Geochim. Cosmochim. Ac.*, 75, 734–752, <https://doi.org/10.1016/j.gca.2010.11.002>, 2011.
- Escobar, J., Hodell, D. A., Brenner, M., Curtis, J. H., Gilli, A., Mueller, A. D., Anselmetti, F. S., Ariztegui, D., Grzesik, D. A., Pérez, L., Schwalb, A., and Guilderson, T. P.: A ~43-ka record of paleoenvironmental change in the Central American lowlands inferred from stable isotopes of lacustrine ostracods, *Quaternary Sci. Rev.*, 37, 92–104, <https://doi.org/10.1016/j.quascirev.2012.01.020>, 2012.
- Gat, J. R., Bowser, C. J., and Kendall, C.: The contribution of evaporation from the Great Lakes to the continental atmosphere: estimate based on stable isotope data, *Geophys. Res. Lett.*, 21, 557–560, 1994.
- Gibson, J., Birks, S., and Edwards, T.: Global prediction of δA and $\delta 2H$ - $\delta^{18}O$ evaporation slopes for lakes and soil water accounting for seasonality, *Global Biogeochem. Cy.*, 22, GB2031, <https://doi.org/10.1029/2007GB002997>, 2008.
- Govender, Y., Cuevas, E., Sternberg, L., and Jury, M.: Temporal variation in stable isotopic composition of rainfall and groundwater in a tropical dry forest in the northeastern Caribbean, *Earth Interact.*, 17, 1–20, 2013.
- Grauel, A.-L., Hodell, D. A., and Bernasconi, S. M.: Quantitative estimates of tropical temperature change in lowland Central America during the last 42 ka, *Earth Planet. Sc. Lett.*, 438, 37–46, <https://doi.org/10.1016/j.epsl.2016.01.001>, 2016.
- Griffiths, M. L., Drysdale, R. N., Vonhof, H. B., Gagan, M. K., Zhao, J.-x., Ayliffe, L. K., Hantoro, W. S., Hellstrom, J. C., Cartwright, I., and Frisia, S.: Younger Dryas–Holocene temperature and rainfall history of southern Indonesia from $\delta^{18}O$ in speleothem calcite and fluid inclusions, *Earth Planet. Sc. Lett.*, 295, 30–36, 2010.
- Guo, W. and Zhou, C.: Triple oxygen isotope fractionation in the DIC-H₂O-CO₂ system: A numerical framework and its implications, *Geochim. Cosmochim. Ac.*, 246, 541–564, 2019.
- Hagen, S. and Keigwin, L. D.: Sea-surface temperature variability and deep water reorganisation in the subtropical North Atlantic during Isotope Stage 2–4, *Mar. Geol.*, 189, 145–162, 2002.
- Hansen, M., Scholz, D., Schöne, B. R., and Spötl, C.: Simulating speleothem growth in the laboratory: Determination of the stable isotope fractionation ($\delta^{13}C$ and $\delta^{18}O$) between H₂O, DIC and CaCO₃, *Chem. Geol.*, 509, 20–44, 2019.
- Hemmer, B.: bhemmer/IsoFluid: v.1.0.0 (v.1.0.0), Zenodo [code], <https://doi.org/10.5281/zenodo.5911265>, 2022.
- Hu, H.-Y., Bao, W.-M., Wang, T., and Qu, S.-M.: Experimental study on stable isotopic fractionation of evaporating water under varying temperature, *Water Science and Engineering*, 2, 11–18, 2009.
- Johnston, V. E., Borsato, A., Spötl, C., Frisia, S., and Miorandi, R.: Stable isotopes in caves over altitudinal gradients: fractionation behaviour and inferences for speleothem sensitivity to climate change, *Clim. Past*, 9, 99–118, <https://doi.org/10.5194/cp-9-99-2013>, 2013.
- Kim, S.-T. and O’Neil, J. R.: Equilibrium and nonequilibrium oxygen isotope effects in synthetic carbonates, *Geochim. Cosmochim. Ac.*, 61, 3461–3475, 1997.
- Lachniet, M. S.: Climatic and environmental controls on speleothem oxygen-isotope values, *Quaternary Sci. Rev.*, 28, 412–432, <https://doi.org/10.1016/j.quascirev.2008.10.021>, 2009.
- Lachniet, M. S. and Patterson, W. P.: Oxygen isotope values of precipitation and surface waters in northern Central America (Belize and Guatemala) are dominated by temperature and amount effects, *Earth Planet. Sc. Lett.*, 284, 435–446, <https://doi.org/10.1016/j.epsl.2009.05.010>, 2009.
- Lases-Hernandez, F., Medina-Elizalde, M., Burns, S., and DeCesare, M.: Long-term monitoring of drip water and groundwater stable isotopic variability in the Yucatán Peninsula: Implications for recharge and speleothem rainfall reconstruction, *Geochim. Cosmochim. Ac.*, 246, 41–59, 2019.
- Lases-Hernandez, F., Medina-Elizalde, M., and Frappier, A. B.: Drip water $\delta^{18}O$ variability in the northeastern Yucatán Peninsula, Mexico: Implications for tropical cyclone detection and rainfall reconstruction from speleothems, *Geochim. Cosmochim. Ac.*, 285, 237–256, <https://doi.org/10.1016/j.gca.2020.07.008>, 2020.
- Lea, D. W., Pak, D. K., Peterson, L. C., and Hughen, K. A.: Synchronicity of tropical and high-latitude Atlantic temperatures over the last glacial termination, *Science*, 301, 1361–1364, <https://doi.org/10.1126/science.1088470>, 2003.

- Lozano-García, S., Ortega, B., Roy, P. D., Beramendi-Orosco, L., and Caballero, M.: Climatic variability in the northern sector of the American tropics since the latest MIS 3, *Quaternary Res.*, 84, 262–271, 2015.
- Lynch-Stieglitz, J., Schmidt, M. W., Henry, L. G., Curry, W. B., Skinner, L. C., Mulitza, S., Zhang, R., and Chang, P.: Muted change in Atlantic overturning circulation over some glacial-aged Heinrich events, *Nat. Geosci.*, 7, 144–150, <https://doi.org/10.1038/Ngeo2045>, 2014.
- Meckler, A. N., Affolter, S., Dublyansky, Y. V., Krüger, Y., Vogel, N., Bernasconi, S. M., Frenz, M., Kipfer, R., Leuenberger, M., and Spötl, C.: Glacial–interglacial temperature change in the tropical West Pacific: A comparison of stalagmite-based paleothermometers, *Quaternary Sci. Rev.*, 127, 90–116, 2015.
- Medina-Elizalde, M., Burns, S. J., Lea, D. W., Asmerom, Y., von Gunten, L., Polyak, V., Vuille, M., and Karmalkar, A.: High resolution stalagmite climate record from the Yucatán Peninsula spanning the Maya terminal classic period, *Earth Planet. Sc. Lett.*, 298, 255–262, <https://doi.org/10.1016/j.epsl.2010.08.016>, 2010.
- Miller, T. E.: Stream Pirates of the Caribbean: Tanamá and Camuy Rivers in the Northern Karst of Puerto Rico, *Espelorevista Puerto Rico*, 2, 8–13, 2010.
- Millo, C., Strikis, N. M., Vonhof, H. B., Deininger, M., da Cruz Jr., F. W., Wang, X., Cheng, H., and Edwards, R. L.: Last glacial and Holocene stable isotope record of fossil dripwater from subtropical Brazil based on analysis of fluid inclusions in stalagmites, *Chem. Geol.*, 468, 84–96, 2017.
- Mühlinghaus, C., Scholz, D., and Mangini, A.: Modelling stalagmite growth and $\delta^{13}\text{C}$ as a function of drip interval and temperature, *Geochim. Cosmochim. Ac.*, 71, 2780–2790, <https://doi.org/10.1016/j.gca.2007.03.018>, 2007.
- Nehme, C., Kluge, T., Verheyden, S., Nader, F., Charalambidou, I., Weissbach, T., Gucel, S., Cheng, H., Edwards, R. L., Satterfield, L., Eiche, E., and Claeys, P.: Speleothem record from Pentadactylos cave (Cyprus): new insights into climatic variations during MIS 6 and MIS 5 in the Eastern Mediterranean, *Quaternary Sci. Rev.*, 250, 106663, <https://doi.org/10.1016/j.quascirev.2020.106663>, 2020.
- Peterson, L. C., Haug, G. H., Hughen, K. A., and Rohl, U.: Rapid changes in the hydrologic cycle of the tropical Atlantic during the last glacial, *Science*, 290, 1947–1951, <https://doi.org/10.1126/science.290.5498.1947>, 2000.
- Putman, A. L., Fiorella, R. P., Bowen, G. J., and Cai, Z.: A Global Perspective on Local Meteoric Water Lines: Meta-analytic Insight Into Fundamental Controls and Practical Constraints, *Water Resour. Res.*, 55, 6896–6910, <https://doi.org/10.1029/2019WR025181>, 2019.
- Rama-Corredor, O., Martrat, B., Grimalt, J. O., López-Otalvaro, G. E., Flores, J. A., and Sierro, F.: Parallelisms between sea surface temperature changes in the western tropical Atlantic (Guiana Basin) and high latitude climate signals over the last 140 000 years, *Clim. Past*, 11, 1297–1311, <https://doi.org/10.5194/cp-11-1297-2015>, 2015.
- Royer, A., Malaizé, B., Lécuyer, C., Queffelec, A., Charlier, K., Caley, T., and Lenoble, A.: A high-resolution temporal record of environmental changes in the Eastern Caribbean (Guadeloupe) from 40 to 10 ka BP, *Quaternary Sci. Rev.*, 155, 198–212, <https://doi.org/10.1016/j.quascirev.2016.11.010>, 2017.
- Sachs, J. P. and Lehman, S. J.: Subtropical North Atlantic Temperatures 60 000 to 30 000 Years Ago, *Science*, 286, 756–759, <https://doi.org/10.1126/science.286.5440.756>, 1999.
- Schmidt, M. W. and Spero, H. J.: Meridional shifts in the marine ITCZ and the tropical hydrologic cycle over the last three glacial cycles, *Paleoceanography*, 26, PA1206, <https://doi.org/10.1029/2010pa001976>, 2011.
- Schmidt, M. W., Vautravers, M. J., and Spero, H. J.: Rapid subtropical North Atlantic salinity oscillations across Dansgaard–Oeschger cycles, *Nature*, 443, 561–564, 2006a.
- Schmidt, M. W., Vautravers, M. J., and Spero, H. J.: Western Caribbean sea surface temperatures during the late Quaternary, *Geochem. Geophys. Geosy.*, 7, Q02P10, <https://doi.org/10.1029/2005gc000957>, 2006b.
- Scholl, M., Torres-Sanchez, A., and Rosario-Torres, M.: Stable isotope ($\delta^{18}\text{O}$ and $\delta^2\text{H}$) values for precipitation, stream water and groundwater in Puerto Rico, *US Geol. Surv. Open File Rep.*, 1011, 25, <https://doi.org/10.3133/ofr20141101>, 2014.
- Scholl, M. A. and Murphy, S. F.: Precipitation isotopes link regional climate patterns to water supply in a tropical mountain forest, eastern Puerto Rico, *Water Resour. Res.*, 50, 4305–4322, <https://doi.org/10.1002/2013wr014413>, 2014.
- Scholz, D., Mühlinghaus, C., and Mangini, A.: Modelling $\delta^{13}\text{C}$ and $\delta^{18}\text{O}$ in the solution layer on stalagmite surfaces, *Geochim. Cosmochim. Ac.*, 73, 2592–2602, <https://doi.org/10.1016/j.gca.2009.02.015>, 2009.
- Schwarcz, H. P., Harmon, R. S., Thompson, P., and Ford, D. C.: Stable Isotope Studies of Fluid Inclusions in Speleothems and Their Paleoclimatic Significance, *Geochim. Cosmochim. Ac.*, 40, 657–665, [https://doi.org/10.1016/0016-7037\(76\)90111-3](https://doi.org/10.1016/0016-7037(76)90111-3), 1976.
- Svendsen, J. I., Alexanderson, H., Astakhov, V. I., Demidov, I., Dowdeswell, J. A., Funder, S., Gataullin, V., Henriksen, M., Hjort, C., and Houmark-Nielsen, M.: Late Quaternary ice sheet history of northern Eurasia, *Quaternary Sci. Rev.*, 23, 1229–1271, 2004.
- Them II, T. R., Schmidt, M. W., and Lynch-Stieglitz, J.: Millennial-scale tropical atmospheric and Atlantic Ocean circulation change from the Last Glacial Maximum and Marine Isotope Stage 3, *Earth Planet. Sc. Lett.*, 427, 47–56, <https://doi.org/10.1016/j.epsl.2015.06.062>, 2015.
- Tremaine, D. M., Froelich, P. N., and Wang, Y.: Speleothem calcite formed in situ: modern calibration of $\delta^{18}\text{O}$ and $\delta^{13}\text{C}$ paleoclimate proxies in a continuously-monitored natural cave system, *Geochim. Cosmochim. Ac.*, 75, 4929–4950, 2011.
- Uemura, R., Kina, Y., Shen, C.-C., and Omine, K.: Experimental evaluation of oxygen isotopic exchange between inclusion water and host calcite in speleothems, *Clim. Past*, 16, 17–27, <https://doi.org/10.5194/cp-16-17-2020>, 2020.
- van Beynen, P., Polk, J. S., Asmerom, Y., and Polyak, V.: Late Pleistocene and mid-Holocene climate change derived from a Florida speleothem, *Quatern.Int.*, 449, 75–82, <https://doi.org/10.1016/j.quaint.2017.05.008>, 2017.
- van Breukelen, M. R., Vonhof, H. B., Hellstrom, J. C., Wester, W. C. G., and Kroon, D.: Fossil dripwater in stalagmites reveals Holocene temperature and rainfall variation in Amazonia, *Earth Planet. Sc. Lett.*, 275, 54–60, <https://doi.org/10.1016/j.epsl.2008.07.060>, 2008.
- Van Meerbeeck, C. J., Renssen, H., and Roche, D. M.: How did Marine Isotope Stage 3 and Last Glacial Maximum climates dif-

- fer? – Perspectives from equilibrium simulations, *Clim. Past*, 5, 33–51, <https://doi.org/10.5194/cp-5-33-2009>, 2009.
- Vieten, R., Winter, A., Warken, S. F., Schröder-Ritzrau, A., Miller, T. E., and Scholz, D.: Seasonal temperature variations controlling cave ventilation processes in Cueva Larga, Puerto Rico, *Int. J. Speleol.*, 45, 259–273, <https://doi.org/10.5038/1827-806x.45.3.1983>, 2016.
- Vieten, R., Warken, S., Winter, A., Scholz, D., Miller, T., Spötl, C., and Schröder-Ritzrau, A.: Monitoring of Cueva Larga, Puerto Rico – A First Step to Decode Speleothem Climate Records, in: *Karst Groundwater Contamination and Public Health*, edited by: White, W. B., Herman, J. S., Herman, E. K., and Rutigliano, M., *Advances in Karst Science*, Springer International Publishing, Cham, 319–331, https://doi.org/10.1007/978-3-319-51070-5_36, 2018a.
- Vieten, R., Warken, S., Winter, A., Schröder-Ritzrau, A., Scholz, D., and Spötl, C.: Hurricane Impact on Seepage Water in Larga Cave, Puerto Rico, *J. Geophys. Res.-Biogeo.*, 123, 879–888, <https://doi.org/10.1002/2017jg004218>, 2018b.
- Warken, S. F., Scholz, D., Spötl, C., Jochum, K. P., Pajón, J. M., Bahr, A., and Mangini, A.: Caribbean hydroclimate and vegetation history across the last glacial period, *Quaternary Sci. Rev.*, 218, 75–90, 2019.
- Warken, S. F., Vieten, R., Winter, A., Spötl, C., Miller, T. E., Jochum, K. P., Schröder-Ritzrau, A., Mangini, A., and Scholz, D.: Persistent Link Between Caribbean Precipitation and Atlantic Ocean Circulation During the Last Glacial Revealed by a Speleothem Record From Puerto Rico, *Paleoceanography and Paleoclimatology*, 35, e2020PA003944, <https://doi.org/10.1029/2020PA003944>, 2020.
- Weber, M., Hinz, Y., Schöne, B. R., Jochum, K. P., Hoffmann, D., Spötl, C., Riechelmann, D. F., and Scholz, D.: Opposite Trends in Holocene Speleothem Proxy Records From Two Neighboring Caves in Germany: A Multi-Proxy Evaluation, *Front. Earth Sci.*, 9, 642651, <https://doi.org/10.3389/feart.2021.642651>, 2021.
- Weißbach, T.: Spectroscopic isotope ratio analysis on speleothem fluid inclusions-analytically and paleoclimatic case studies, Dissertation, Institute of Environmental Physics, Ruprecht-Karls-Universität Heidelberg, Heidelberg, <https://doi.org/10.11588/heidok.00028559>, 2020.
- Winter, A., Zanchettin, D., Lachniet, M., Vieten, R., Pausata, F. S. R., Ljungqvist, F. C., Cheng, H., Edwards, R. L., Miller, T., Rubinetti, S., Rubino, A., and Taricco, C.: Initiation of a stable convective hydroclimatic regime in Central America circa 9000 years BP, *Nat. Commun.*, 11, 716, <https://doi.org/10.1038/s41467-020-14490-y>, 2020.
- Ziegler, M., Nürnberg, D., Karas, C., Tiedemann, R., and Lourens, L. J.: Persistent summer expansion of the Atlantic Warm Pool during glacial abrupt cold events, *Nat. Geosci.*, 1, 601–605, <https://doi.org/10.1038/ngeo277>, 2008.